Transition-Metal Cationization of Laser-Desorbed Perfluorinated Polyethers with FTICR Mass Spectrometry

Evan F. Cromwell,*,‡ Karsten Reihs,† Mattanjah S. de Vries,† Sahba Ghaderi,‡ H. Russell Wendt,† and Heinrich E. Hunziker†

IBM Research Division, 650 Harry Road, San Jose, California 95120-6099, and IBM, 5600 Cottle Road, San Jose, California 95193

Received: October 27, 1992; In Final Form: January 20, 1993

Mass spectra of perfluorinated polyether (PFPE) films on metal substrates have been measured using a novel transition-metal cationization technique combined with FTMS. Full parent mass distributions were obtained with this technique. Two pulsed lasers were employed: a low fluence laser for PFPE desorption and a high fluence laser for metal ion formation. Cationization was observed to occur in the gas phase above the sample surface. The dynamics of the process are discussed. Applications to measure average molecular weights and study photochemistry of PFPE samples are presented. Electron attachment to PFPEs was also studied. Only negative ion fragments were observed from this process.

Introduction

Perfluorinated polyethers (PFPE) are widely used throughout industry as lubricants. Compared to their hydrocarbon analogues, they are more chemically inert and thermally stable, and have very low vapor pressures at room temperature. This makes them particularly attractive for use in harsh environments and areas where polymer degradation is a concern. Two examples of PFPEs, a straight chain (I) and a branched "Y" chain (II) polymer, are shown below. These polymers are commercially available with average molecular weights ranging from 2000 to 10 000.

$$CF_3\text{–}CF_2\text{–}CF_2\text{–}O\text{–}(CF_2\text{–}CF_2\text{–}CF_2\text{–}O)_n\text{–}CF_2\text{–}CF_3 \quad (I)$$

$$CF_3\text{–}CF_2\text{–}CF_2\text{–}O\text{–}(CF(CF_3)\text{–}CF_2\text{–}O)_n\text{–}CF_2\text{–}CF_3 \quad (II)$$

The study of organic polymers by mass spectrometry has been an active field of research in recent years.[1] Both time of flight (TOF) and Fourier transform ion cyclotron resonance mass spectrometry (FTMS)[2] have been used in combination with a variety of ionization methods. The challenge in such studies lies in getting the molecules into the gas phase and ionizing them without fragmentation. Secondary ion mass spectrometry (SIMS),[3] matrix-assisted laser desorption,[4,5] and laser desorption/cationization with alkali salts[6,7] and transition metals[8] have all been successful in this regard with hydrocarbon molecules. However, obtaining mass spectra of PFPEs has been more difficult. Electron impact ionization and SIMS on most surfaces produce only fragment ions. Ag^+ cationized parent mass spectra have been observed from specially prepared surfaces by SIMS.[9]

We report here on our efforts to obtain mass spectra of various PFPE compounds using laser desorption methods coupled with FTMS. The compounds were studied as thin films on metal surfaces. Initial experiments involved laser desorption of the PFPE films combined with attachment of a photoelectron (generated from the metal surface) to create negative PFPE ions. No PFPE parent ions were observed due to efficient decomposition of the negatively charged polymers.

A second method, which used a novel cationization technique, was quite successful at producing parent mass distributions.[10] In this method two lasers were employed, a softly focused laser to desorb the polymer molecules and a tightly focused laser to create a plume of metal ions. The metal ions attach to the desorbed PFPE molecules creating cation complexes. Separation of the desorption and cationization processes allowed independent optimization of the two laser/material interactions. By use of this technique, full parent mass distributions of various PFPE compounds were obtained. Other benefits of this method of cationization are that surface and sample preparation are minimized. Furthermore, samples do not contain dopants for cationization allowing the study of their intrinsic chemistry in situ.

Various experiments were performed to characterize the cationization process and provide insight into the dynamics of the ion–molecule reaction that forms these complexes. In addition, applications of this technique will be discussed. These include measurements of molecular weight distributions and average molecular weights of PFPE samples as well as purity analysis of those compounds. Finally, the use of this technique to study photochemistry of PFPEs will be presented.

Experimental Section

All mass spectra were obtained with a Fourier transform ion cyclotron resonance mass spectrometer (FTMS). The theory and applications of FTMS spectrometry are well established[2,11,12] and will not be discussed here. A schematic of our apparatus is shown in Figure 1. The ion trap (shown in the expanded region of Figure 1) was a standard cubic cage design with inner dimensions 2 in. × 2 in. × 2 in..[13,14] Holes, 6 mm in diameter, were located in the middle of the two trapping plates to provide access to the sample by the lasers and to allow ions from the sample to enter the trap. The trap was centered in the experimental chamber which was pumped by a liquid-nitrogen-trapped diffusion pump and had a base pressure of 8×10^{-9} Torr. The magnetic field was supplied by a superconducting magnet with a 6 in. diameter room temperature bore and a design field of 7 Tesla. For the experiments described here the magnet was run at 4.3 T. When shimmed, the field in the ion trap was homogeneous within ±3 ppm as determined by a NMR probe.

Samples were introduced by attaching them to the tip of an aluminum probe (1 in. diameter) which was inserted into the experimental chamber through a differentially pumped load lock. The distance from the sample surface to the ion trap was adjustable and typically set at 1 mm. The probe was rotatable by 360° and its axis of rotation was offset from the center of the ion trap by 0.25 in. This allowed sampling along an 0.5 in. diameter circle when rotating the probe, giving access to a large portion of the

* Author to whom correspondence should be addressed.
† IBM Research Division, 650 Harry Rd., San Jose, CA.
‡ IBM, 5600 Cottle Rd., San Jose, CA.

0022-3654/93/2097-4720$04.00/0

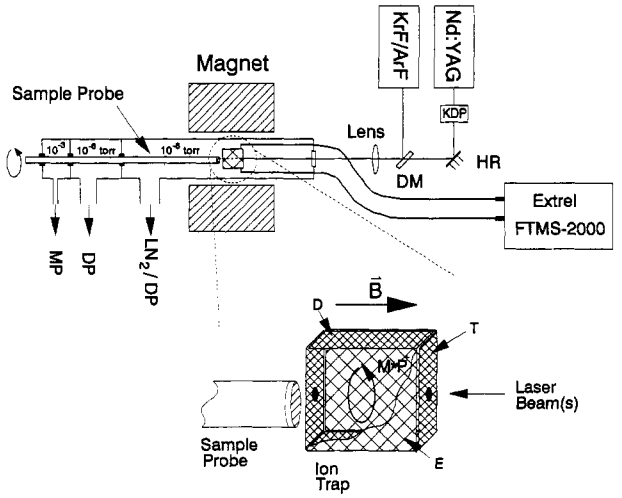

Figure 1. Schematic drawing of the experimental setup (MP = mechanical pump, DP = diffusion pump, DM = dichroic mirror, and HR = high reflectance mirror). The sample/ion trap region is shown in expanded scale (D = detect plate, T = trap plate, E = excite plate, and B = magnetic field).

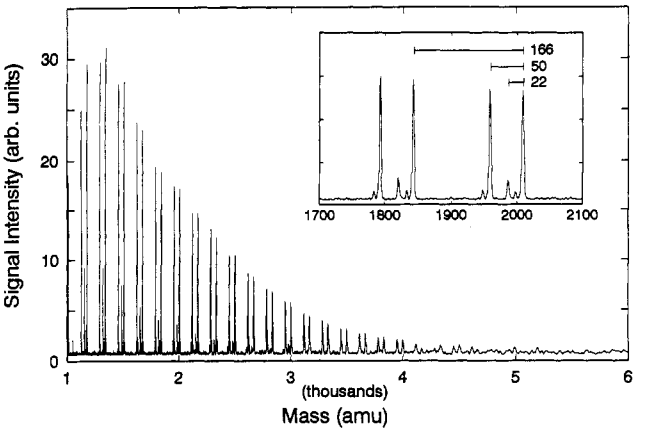

Figure 2. Negative ion spectrum obtained from desorption and electron attachment of a Demnum S-65 PFPE sample ($\langle M \rangle$ = 4600 amu). An expanded view of two peak sets is shown in the insert (mass scale and spacings are in amu).

sample. The probe tip (and hence the sample) was electrically insulated from the rest of the chamber in order to be able to bias the tip with respect to the ion trap.

The ion trap was controlled by an EXTREL FTMS 2000 operating system running on a Nicolet 1280 computer. The trapping voltage was 2 V, its polarity depending on whether positive or negative ions were being detected. The excitation pulse had an amplitude of 80 V peak-to-peak and a duration of <1 ms. Detection time was variable, depending on the mass range and resolution desired, ranging from 3 to 70 ms. The upper limit of the detection time (and hence the resolution) was dictated by the chamber pressure. To achieve better resolution at high masses, the metal ions created during the cationization process were ejected from the trap via the stored waveform inverse Fourier transform (SWIFT) technique.[15] This ejection, which occurred before excitation and detection of the remaining ions, reduced the effects of space charge and ion–ion collisions inside the trap which degrade mass resolution. Unit mass resolution was obtained up to about 1800 amu.

At the start of each experimental sequence the ion trap was quenched (2 ms) and then the desorption and metal ion generation lasers were fired. After a 10-ms delay, the SWIFT ejection and ion excitation rf pulses were applied followed by the ion detection event. One of the lasers (a Nd:YAG) served as the master clock, running at 10 Hz and triggering delay generators that controlled the timing of the other events. Due to the length of each sequence the actual experiment ran at less than 10 Hz. In order to externally trigger the FTMS-2000 system, it was necessary to modify the controller. This modification is described elsewhere.[16]

As mentioned previously, two pulsed lasers were used, one for the PFPE desorption and another for metal ion formation. Typically, 2–4 mJ/pulse of 248-nm light (20 ns fwhm) from a KrF excimer laser (Lumonics EX-400) was softly focused to an elliptical spot with a 2 mm long axis for desorption. To create the metal ions, a 0.3-mJ pulse of 532-nm light (10 ns fwhm) from the doubled output of a Nd:YAG laser (Quanta-Ray GCR-4 with KDP doubling crystal) was tightly focused. The laser beams were overlapped using a 248-nm high reflectance, 45°, dichroic mirror (Acton Research) which transmitted >80% of the 532-nm beam (see Figure 1). The beams were focused by the same nominally 1-m focal length fused silica lens. The difference in laser spot size was achieved by employing the difference in focal length of the lens at 532 and 248 nm. To investigate the effect of wavelength on the desorption process or on PFPE photochemistry, the roles of the two lasers could be reversed by simply moving the lens forward, bringing the excimer instead of the Nd:YAG beam to sharp focus, and adjusting the pulse energies accordingly. In this scenario the molecules would be desorbed by 532-nm radiation. Some experiments were performed using a 193-nm ArF excimer laser (Lumonics EX-400) in place of the KrF laser for desorption.

Commercial samples of the various PFPEs were obtained from Du Pont Co. and Daikin Industries and used without purification. Compounds I and II have the trade names Demnum[17] and Krytox,[18] respectively. Samples were prepared by making ~5% by weight solutions of the PFPEs in *n*-perfluorohexane. A film of the sample was then cast on a clean metal surface by applying a few drops of the solution and letting the solvent evaporate. The metal substrates were prepared by cutting and flattening foils of various metals (typically 0.010 in. thick) to appropriate sizes, cleaning the pieces in successive ultrasonicator baths of Freon and acetone, and attaching the foils to the sample holder with double-sided tape. Surface preparation was not critical because the experiment was not sensitive to PFPE/metal surface interactions since the thickness of the polymer films was on the order of 1 μm.

Results and Discussion

I. Electron Attachment. When a PFPE film on a metal surface is exposed to a UV laser pulse (either 193 or 248 nm) of sufficient intensity, a characteristic set of negative ion peaks is observed. Such a mass spectrum for a Demnum sample (type I, $\langle n \rangle$ = 25) on a Au surface is shown in Figure 2. Only the mass peaks above 1000 amu are shown; all lower mass ions were ejected with a SWIFT waveform for this spectrum. Fall off of the peak intensities below 1200 amu is due to the limited resolution of the SWIFT waveform. The spectrum was taken with 0.5 mJ/pulse of 193-nm light focused to a ~100 μm diameter spot and averaged over six spots on the sample for 500 shots/spot. No positive ions were generated under these conditions.

The spectrum consists of sets of three peaks that repeat every 166 amu. This spacing is equivalent to the mass of the polymer repeat unit. Two of these sets are shown in the insert of Figure 2. The two major peaks are spaced by 50 amu, corresponding to a CF_2 group, while the minor peak is spaced 22 amu from the high mass peak in the group. The origin of this peak will be discussed later. Small ripples on the low mass side of the major peaks, which are spaced by a constant frequency, are artifacts due to "ringing". The intensity of each group grows roughly exponentially toward lower mass. Measurements of the lower masses verified that this trend continues down to $n = 0$. The exponent of this increase is found to depend on the laser energy and wavelength, with higher pulse energies and shorter wavelengths producing a steeper increase.

The two major peaks in each group of the spectrum can be explained by a simple model involving two competing reaction channels. During or after desorption of a polymer molecule, a photoelectron from the metal surface attaches to the polymer causing dissociation via one of two pathways

$$R_1\text{–}(CF_2CF_2CF_2O)_n\text{–}R_2 + e^- \rightarrow R_1\text{–}(CF_2CF_2CF_2O)_x\text{–}CF_2CF_2CF_2O^- + {}^{\bullet}CF_2CF_2CF_2O\text{–}(CF_2CF_2CF_2O)_{n-x-2}\text{–}R_2 \quad (1)$$

$$R_1\text{–}(CF_2CF_2CF_2O)_n\text{–}R_2 + e^- \rightarrow R_1\text{–}(CF_2CF_2CF_2O)_x\text{–}CF_2CF_2CF_2{}^{\bullet} + {}^-OCF_2CF_2CF_2O\text{–}(CF_2CF_2CF_2O)_{n-x-2}\text{–}R_2 \quad (2)$$

where $R_1 = CF_3CF_2CF_2O$– and $R_2 = -CF_2CF_3$. The negative fragment observed carries the $-CF_2CF_2CF_2O^-$ group. The peaks with the 50 amu difference correspond to negative ion fragments with long or short end groups (R_1 or R_2, respectively). The rough equivalency between the intensities of the two peaks indicates that the two channels are equally probable. This same fragmentation pathway has been observed for CF_3–O–CF_3 in the gas phase.[19] In this case electron attachment leads to the formation of $CF_3O^- + CF_3$.

The overall shape of the distribution can be understood by considering that each fragment can undergo further fragmentation. These secondary reactions can result from electron attachment to a neutral fragment or dissociation of a negatively charged fragment. It is possible for electron attachment to occur away from the surface because the photoelectrons are moving much faster than the neutral molecules. The distribution can be modeled by successive random dissociations along the polymer chain. In other words, each $-CF_2$–O–CF_2– center on a negatively charged polymer is equally reactive. When this process is repeated several times, it produces a fragment distribution rising exponentially toward the monomer. Increasing the laser energy increases the number of random breaks. As the number of breaks increases, the distribution gets steeper, being weighted toward shorter chains. This is consistent with experimental observations for higher laser pulse energies and shorter wavelengths.

The possible secondary reactions are important to understanding the negative ion spectrum. The $-CF_2O^-$ end group may dissociate into $-CFO + F^-$. This would create a PFPE with an acid fluoride end group which, upon electron attachment, could form a negative ion according to

$$R_1\text{–}(CF_2CF_2CF_2O)_m\text{–}CF_2CF_2CFO + e^- \rightarrow R_1\text{–}(CF_2CF_2CF_2O)_yCF_2CF_2CF_2{}^{\bullet} + {}^-OCF_2CF_2CF_2O\text{–}(CF_2CF_2CF_2O)_{m-y-2}\text{–}CF_2CF_2CFO \quad (3)$$

accounting for the presence of the third peak in each set (Δm = 22 amu). Another mechanism for formation of a negative ion with a –CFO end group could involve a nucleophilic displacement of an alkoxide by a fluoride as follows:

$$R_1\text{–}(CF_2CF_2CF_2O)_m\text{–}CF_2CF_2CFO + F^- \rightarrow R_1\text{–}(CF_2CF_2CF_2O)_yCF_2CF_2CF_3 + {}^-OCF_2CF_2CF_2O\text{–}(CF_2CF_2CF_2O)_{m-y-2}\text{–}CF_2CF_2CFO \quad (4)$$

For CF_3–O–CF_3 this reaction is predicted to be exothermic by 1.6 eV from the data of Spyrou et al.[19] The F^- can also react with the $-{}^{\bullet}CF_2-$ radical end group exothermally ($\Delta H \sim 2$ eV) and with a small barrier (0.1 eV), to give $CF_3^- + e^-$.[20] This leads to formation of a shorter chain PFPE (with the same end groups as the parent) which can undergo further decomposition by the mechanisms described above. This reaction is important in limiting the types of fragments observed. A small peak, 19 amu lower than the main peaks, is also present in the lower mass peak sets (it is not resolved in the insert in Figure 2). It is possible that some PFPEs with $-{}^{\bullet}CF_2$ end groups undergo electron attachment and subsequent dissociation before reacting with F^-, thus accounting for the presence of those peaks. Under higher laser fluences additional fragment types are seen, especially in the low mass region (<1000 amu), although the progression discussed above is still observed. The origins of these ions will not be discussed here. It is not possible to determine from these results whether the polymer fragmentation occurs in the liquid film or in a gas-phase, high-density region above the surface. In previous work by Pacansky et al.,[21] acid fluorides were observed in PFPE films after bombardment by high-energy electrons suggesting that fragmentation might be occurring in the condensed phase.

Negative ions corresponding to parent PFPE molecules were searched for extensively at many different laser fluences, at 248 nm as well as 193 nm desorption wavelengths, with various PFPE film thicknesses, and with different metal substrates. No such ions were ever observed. This suggests that the barrier to dissociation of the negatively charged polymers is very low. Therefore, after electron attachment, the rate of polymer dissociation is much greater than that of negative ion stabilization under the conditions of our experiment. We also observed that the extent of fragmentation decreased at longer desorption wavelengths and detected no negative ions at 532 nm under low laser fluence conditions. This can be attributed to insufficient photon energy to generate photoelectrons from the substrate.

II. Cationization. Cationization, particularly by alkali metals, has been used in mass spectrometry for over 10 years.[6,22] However, this method requires the introduction of large amounts of salt into a sample and generally has the disadvantage of requiring significant sample preparation. We were unable to obtain cationized spectra of PFPEs by this method. As an alternative we developed a transition-metal cationization scheme which utilizes two lasers to separate the desorption and cationization steps and allows for independent optimization of each process. Under appropriate conditions, neither laser alone produces cationized molecules. Separation of the desorption and cationization processes has been demonstrated previously, but with a single laser.[23,24] The benefits of using two separate lasers are significant and will be addressed below. In part A of this section some of the aspects of the laser/material interactions that pertain to the cationization process will be discussed. In part B experiments undertaken to elucidate the chemistry and physics of the cationization process will be described. Parts C and D present applications of the technique to determine molecular weight distributions and photochemical degradation products.

A. Desorption/Ablation Dynamics. There has been a wealth of information published on laser desorption and laser ablation of polymers.[25,26] It is not the purpose of this paper to describe the laser/material interaction in detail. However, the use of two lasers made possible certain experiments concerning this subject. Here, for the sake of clarity, we refer to the PFPE vaporization as "desorption" and the metal ion formation as "ablation" although the actual mechanisms of the processes are not completely understood. The information from these studies helps to characterize the role of the desorption and ablation in the cationization process.

The spot size of the laser used to create the metal ions was much smaller than the spot size of the laser used to desorb the PFPE. The reason for this is that the laser fluence necessary to create the metal ions causes fragmentation of the PFPEs. On the other hand, at lower laser fluences, where PFPE desorption occurs without excessive fragmentation, no metal ions are created. Thus the two processes must necessarily be separated. The gaseous PFPE molecules and metal ions created by the two lasers combine above the surface and form the polymer/metal cation complexes.

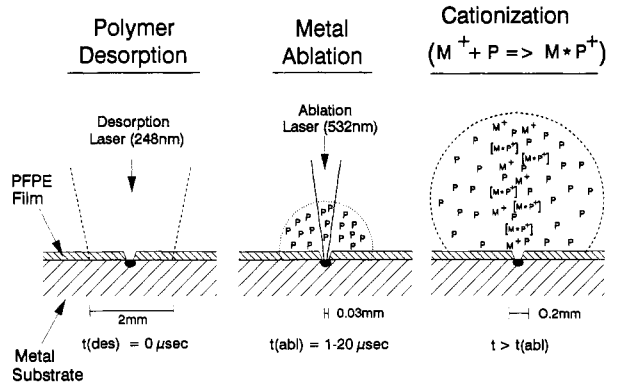

Figure 3. Diagram of the laser/sample interactions and the cationization process (not to scale). Shown, left to right, are polymer desorption, metal ablation, and cationization (P = polymer molecule, M^+ = metal ion, M^*P^+ = cation complex). The approximate widths of the desorption beam, the ablation beam, and the interaction region and the timing of the desorption, ablation, and cationization events are given beneath the drawing.

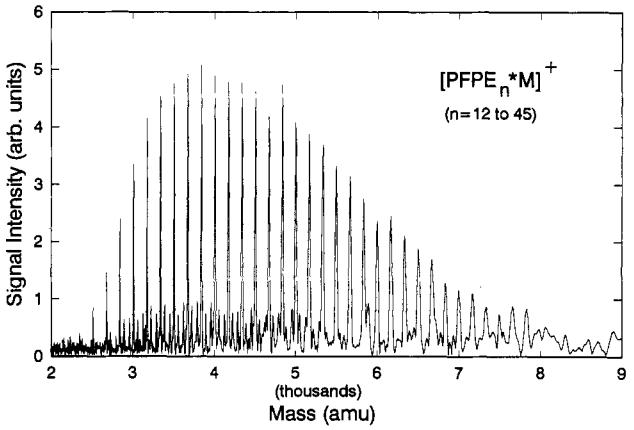

Figure 4. Mass spectrum of cationized Demnum S-65, having structure I and $\langle M \rangle$ = 4600 amu. The PFPE film was on a Au/Ni coated Cu sample. The desorbed polymer was cationized by Ni^+.

A diagram of the complete process is shown in Figure 3. A representative mass spectrum obtained by this method is shown in Figure 4.

In order to investigate the dynamics of the desorption process, we varied the time delay between the PFPE desorption laser and the metal ablation laser. The experiment was performed with a sample of the Y-chain polymer (II) with average molecular weight $\langle M \rangle$ = 4000, deposited on a Cu foil. The intensity of the cation complex signal was normalized to the Cu^+ ion signal. The results of this are shown in Figure 5.

The most striking aspect of Figure 5 is the asymmetry of the intensity versus time delay curves. While cationization is observed for PFPE desorption preceding metal ion generation by over 20 μs, the signal disappears if the metal ions are formed more than 1 μs before desorption occurs. Two effects are possibly responsible for this behavior: a difference in the time duration of the two processes and the relative velocity of the species involved. Ablation of polymers[27] and "pressure pulse" desorption of liquid layers[28] have been seen to extend for many microseconds after the laser light is gone. The metal ion formation, on the other hand, is expected to be very short, on the order of 1 μs or less.[29] Thus cationization can occur over an extended period only if the desorption comes first. The second effect can be understood as follows: if the PFPE molecules and the metal ions were to come off at the same temperature, the polymers would move around 5 to 10 times slower because of their heavier mass. The metal ions are expected to have higher kinetic energies than the PFPEs making this difference even larger. Thus the metal ions can catch up with the PFPE molecules, while the reverse is not possible,

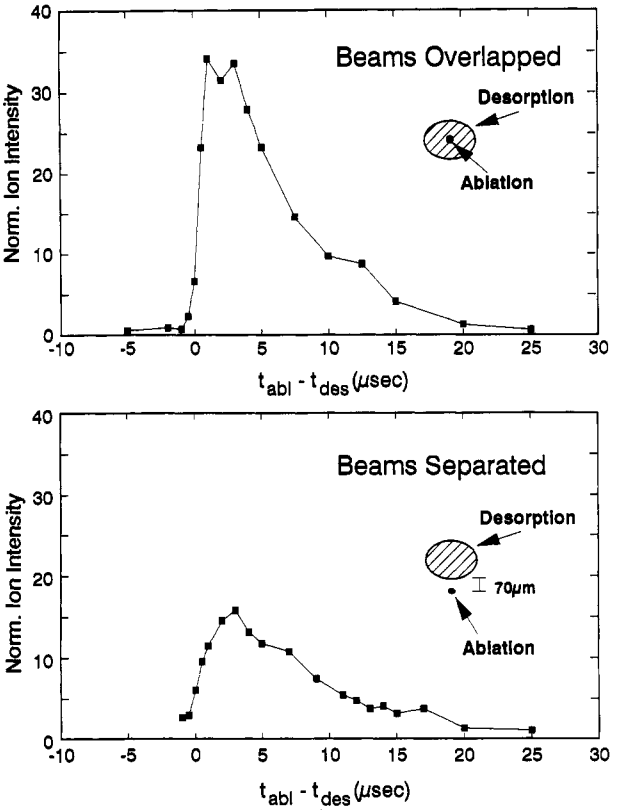

Figure 5. Cationized PFPE signal intensity as a function of the delay between the desorption and metal ablation lasers (positive delay corresponds to desorption occurring first): top trace, spatially overlapped lasers; bottom trace, 70 μm separation between center of the ablation laser and the edge of the desorption area. The signals, Cu^+ cationized Krytox 24 (type II, $\langle M \rangle$ = 4000 amu), are normalized to the Cu^+ intensity. The desorption and ablation beams have widths of 2 mm and 30 μm, respectively. The drawings show relative positioning of the two beams.

leading to asymmetry in the time delay curve. Given our experimental setup it would be difficult to deconvolute these two effects since they are interdependent.

A related experiment addressed the effect of spatial separation of the two lasers on the cationization signal. The relative position of the laser beams was determined by taking a burn spot of the two lasers, external to the vacuum chamber, at a distance from the lens equivalent to the distance to the sample surface. At zero time delay the signal remained relatively constant as long as the two spots overlapped. As the spots were separated, the signal (at $t = 0$) decreased until it disappeared at a separation of ~200 μm between the center of the ablation spot and the edge of the desorption area. A time delay trace, measured with the laser separation at 70 μm, is shown in Figure 5b.

The peak of the signal for the separated lasers is shifted by 1 to 2 μs from that of the overlapped lasers. This delay can be related to the time necessary for the PFPE molecules to move into the plume of metal ions which is confined to move perpendicular to the surface by the magnetic field. In addition to the timing change the signal decreased by approximately a factor of 2. This is attributed to reduced overlap between the metal ion and PFPE plumes. The time delay curves are affected more strongly at early delays because the PFPE cloud is still relatively small making the fast metal ions miss a large fraction of that cloud. At later delays, the PFPEs have spread out more so the initial location of the metal ions does not have as strong an effect on the cation signal.

Two other aspects of the desorption/cationization process merit discussion.

(1) The cationization process is observed only for a narrow range of ablation laser pulse energies (0.25–0.32 mJ at 532 nm). Two possible explanations are offered here. As ablation energy

is increased the velocity of the material expansion increases[28] giving the metal ions a larger kinetic energy. It has been observed that the cross section for the reaction of metal ions with C_2F_4 is strongly dependent on the relative kinetic energy of the reactants[30] with a "bell shaped" response. Assuming that the behavior for PFPE cationization is similar, the range of laser energies given above could possibly correspond to the range of metal ion kinetic energies where the cationization cross section is largest. Another question is what role excited electronic states of the metal ions play in the cationization process. An increase in metal ablation energy will be accompanied by an increase in the populations of those states possibly affecting the cationization efficiency.

(2) In thermally induced laser desorption a sharp temperature jump at the surface caused by absorption of the laser radiation is thought to be the driving force behind the desorption event. Such a mechanism describes the desorption of monolayer coverages of organics well. However, vaporization of PFPEs from a thick film cannot be described in this manner because the film does not absorb at the wavelengths used for desorption. Furthermore, the thermal conductivity of the metal substrate, at whose surface the light is absorbed, is much greater than that of the PFPE film. Thus while the metal is expected to heat up rapidly and experience a large temperature jump, the temperature of the PFPE, especially at the film/vacuum interface, should remain relatively low.

A more likely mechanism may be the following: At the metal/PFPE interface the absorption of the laser radiation produces a sudden vaporization of the PFPE film. This, in turn, causes a pressure wave to move through the liquid PFPE layer and eject material when it reaches the PFPE/vacuum interface. With this mechanism the PFPE molecules are not excessively heated, and so thermal fragmentation of the polymer is minimized. The laser flux can be adjusted to achieve an almost constant desorption intensity from a single spot extending over several hundred successive pulses.

Metal ion formation occurs by a different process. The tightly focused laser beam causes a localized plasma to form creating numerous ions. The plume of ions will be directional, moving perpendicularly to the surface, due to the high magnetic field. The ions will also move rapidly, due to the high gas temperature. We noted that the number of metal ions produced by the first few laser shots was lower than the "steady state" intensity. This can be understood as a consequence of the presence of the PFPE layer, which initially inhibits the ion flux but is quickly ablated away.

B. Cationization Dynamics. The evidence presented above supports a gas-phase cationization process. This is similar to cationization with Na and K salts which has been documented as occurring in the gas phase.[23,24] However, the dynamics of these processes are not well understood. A key question is whether the complex is bound by an electrostatic interaction or whether the transition-metal ions oxidatively add to the CF, CC, or CO bonds. Extensive reviews of gas-phase transition-metal chemistry have been published[31,32] covering the reactions of metal ions of known kinetic energy with various alkanes, alcohols, and ethers[33,34] and with perfluorinated compounds.[30] In all these studies metal ion addition is accompanied by fragmentation. However, in the cationization process explored here no fragmentation of the parent PFPEs is observed. This supports an electrostatic bond between the metal ions and the parent polymers. There is evidence that oxidative addition also occurs (with polymer fragmentation) and will be discussed later. Some understanding of the dynamics of the cationization of PFPEs can be gained from the present studies by examining various combinations of different polymers and metal ions. In particular, given the repetitive nature of the polymers, one can view the cationization complexation reaction as occurring either at a polymer end group or along a repeat unit and address the role of these groups in the cationization process.

(a) Effect of End Groups. In order to study the role of end groups, straight chain polymers with the following terminations were examined:

$$CF_2CF_2CF_2O\text{–}(CF_2CF_2CF_2O)_n\text{–}X$$

$$X = CF_2\text{–}CF_3 \qquad \text{(I)}$$

$$X = CF_2\text{–}CF_2\text{–}COO\text{–}(CH_2\text{–}CH_2\text{–}O\text{–}C_6H_5) \qquad \text{(III)}$$

$$X = CF_2\text{–}CF_2\text{–}CH_2\text{–}OH \qquad \text{(IV)}$$

Due to the method used to make the polymer derivatives, samples of derivatives III through IV contained about 30% of unaltered polymer (I). This fact was exploited to study the effect of the PFPE end group on the cationization efficiency.

A comparison of the cation complex signal for molecules with similar length but different end groups in a sample will give an indication of the relative cationization efficiencies of polymers containing those end groups. No difference in cationization efficiency was seen for polymers with different end groups within the limits of the experiment. This implies that the metal ions are attaching predominantly to the repeat units and not to the end groups. Additional support for this conclusion comes from the proportionality of cationization efficiency and chain length, discussed in subsection C.

(b) Effect of Repeat Units. The effect of varying the repeat unit was studied by comparing the cationization efficiencies of straight and Y-chain polymer samples (shown above as I and II, respectively). We assumed that the desorption efficiency for two polymer molecules with isomeric repeat units and equal mass would be about the same. Since the polymers are isomers, and thus their mass spectra coincide, it was necessary to put the samples on two separate Cu foil pieces on the same sample holder. To account for changes in experimental conditions between the two samples, a lower molecular weight polymer was added as an internal standard. This was a type I polymer with an average molecular weight of 2000, added to the polymer solutions in a 1:4 weight ratio (low molecular weight polymer:high molecular weight polymer).

Two mass spectra from this measurement are shown in Figure 6. The bottom trace shows a mixture of two straight chain polymer samples with $\langle M \rangle = 4600$ and $\langle M \rangle = 2000$. The top trace shows a mixture of a Y-chain polymer sample ($\langle M \rangle = 4000$) and, again, the $\langle M \rangle = 2000$ reference polymer. A dramatic difference can be seen between the two spectra. The relative abundance of the high molecular weight portions of the two different samples can be deduced by first determining the relative abundance of high and low molecular weight portions within the same sample and then using the weight ratio of the two mixtures for normalization. Peaks between 2300 and 2700 amu were not used because of overlap between the low and high mass components. The ratio between the normalized peak areas of equivalent mass (averaged over five spectra) was then calculated. The Y polymer was observed to cationize 5 ± 1 times as efficiently as the straight polymer.

We have considered several different explanations for the large difference between cationization efficiencies of branched (II) versus unbranched (I) PFPE structures. For this discussion it is helpful to refer to the Mulliken net charge on each atom calculated for two related model compounds with the Gaussian 86 SCF program, shown in Figure 7.[35] Because of the large negative charge on the ether oxygen it is tempting to postulate that cationization occurs at this site. However, our observations do not confirm such a notion. Space-filling models show the oxygen to be more sterically shielded for the branched structure. This should result in a smaller reaction probability, as has been observed for Lewis acid attack,[36] while we observe a higher cationization

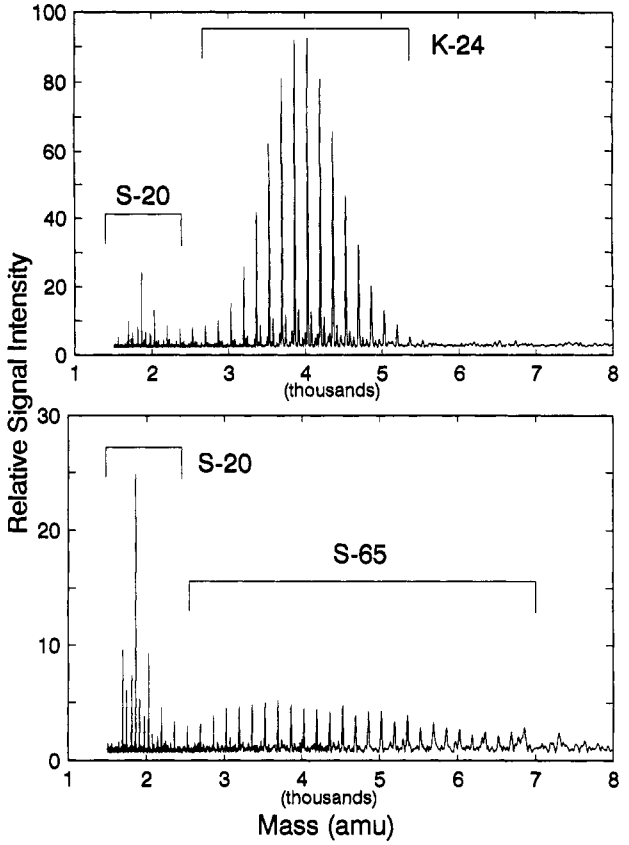

Figure 6. Spectra showing the relative cationization efficiency of straight chain versus Y chain PFPEs: top trace, mixture of Demnum S-20 and Krytox 24; bottom trace, mixture of Demnum S-20 and Demnum S-65. Mixtures contain approximately 20% (by weight) of S-20. The signal intensities have been scaled to the Demnum S-20 distributions.

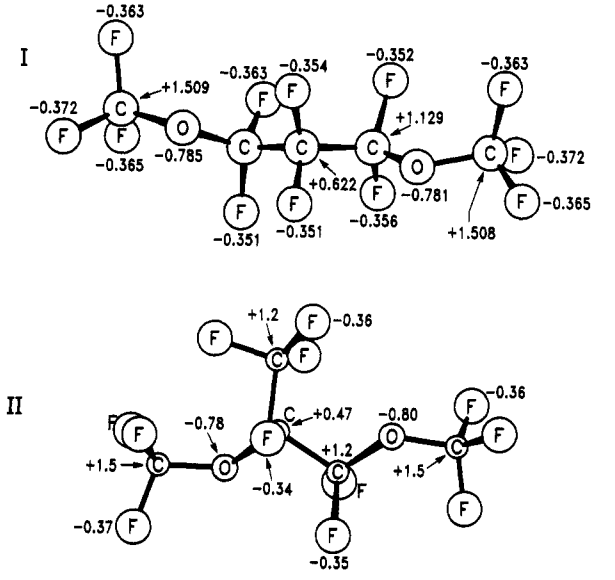

Figure 7. Mulliken net charges per atom for models of PFPEs I and II as calculated with the Gaussian 86 SCF program (from ref 35).

efficiency for the branched structure. Also, by cationizing n–$C_{20}F_{42}$ we found that straight perfluoroparaffins cationize just as efficiently by our method as do PFPEs.

Another explanation could be conceived based on the enhancement of the observed cross section by the presence of CF_3 groups, by postulating a specific interaction of the metal ion with the three negatively charged F atoms. However this model fails because at reasonable distances the electrostatic interaction is always repulsive, due to the net positive charge of the CF_3 group (as determined from adding up the net atomic charges shown in Figure 7).

A more attractive picture can be based on the fact that cationization cross sections are known to depend primarily on polarization and dipole interactions.[37,38] This can be understood in terms of a double well potential curve along the reaction coordinate.[39] The outer well corresponds to an electrostatic interaction, or an initial complex formation, while the inner one corresponds to chemical bonding (which may or may not occur). The polarizability and dipole strength affect the stability of the initial complex. The polarizabilities of PFPEs are quite low as indicated by their dielectric constant ($\epsilon \sim 1.7$). There is, however, a pronounced difference in the dipole moment of the repeat units as estimated from the net atomic charges of Figure 7. For the branched structure it is about 1.2 D while for the unbranched one it is essentially zero. The negative end of the dipole in the branched structure is approximately opposite the CF_3 group. Thus the local dipoles of the branched polymer chain may give it a larger cross section for cationization and a deeper electrostatic potential well which reduces the probability of redissociation. Both effects can increase the overall cationization efficiency.

(c) Effect of Different Metals. In addition to varying the polymer compositions as described above, we also examined the effect of the type of metal ion used. This was done by varying the metal substrate that the PFPE film was deposited on. We used the following pure metal foils: Cu, Ni, Fe, Co, Ti, Mo, Ta, Ag, Mn, Al, and Au. Several alloys were used as well to study relative cationization efficiencies. These included Ni/Cr (Nichrome), Cu/Ni (Constantan), and Cu/Zn (brass). All metals were observed to cationize the PFPEs except for Au.

It is difficult to draw any quantitative conclusions from these studies because the kinetic energies of the metal ions are not known and the complex formation cross sections may depend on those energies. By comparing the cationized PFPE signal strength to the metal ion signal intensity, it appeared that the row 4 transition metals (Cr, Fe, Ni, Co, Cu, Zn) were the most efficient as a group at cationizing the desorbed polymer. Some metals (Mo in particular) required slightly higher ablation energies in order to produce significant amounts of metal ions. This may be related to higher ablation thresholds for those materials. Ag, which has been found to cationize efficiently via TOF-SIMS,[9] appeared to be less efficient than the row 4 elements in our experiments.

Several alloys of row 4 transition metals were used in order to make a more direct comparison of relative cationization efficiencies. Figure 8 compares typical signals observed for Cu and Ni ions ablated from Constantan (45% Ni, 55% Cu) to the cationized PFPE (n = 11) signal observed for polymer desorbed from that alloy. As can be seen, the ratio of the different cation complexes closely follows that of the metal ions indicating that the cationization cross section for these two metals is roughly equivalent. Similar behavior was observed for the other alloys studied (Ni/Cr and Cu/Zn). It thus appears that cationization efficiency for row 4 metal ions is fairly constant. This is to be expected if the interaction leading to cationization is electrostatic.

Generally, a small amount of positive polymer fragment ions can be observed during the laser cationization process, particularly at higher desorption laser fluence. We found a difference in the amount and intensity of fragment ions observed from cationization with certain metals. With Fe and Zn in particular, peaks corresponding to metal/polymer fragment cations appeared in the mass spectra. In previous reports of reactions of metal ions with alkanes, ethers, and ketones,[40,41] it was noted that Fe was more reactive than other row 4 transition metals and led to a wider array of products. This was explained by the fact that the oxidative addition of Fe^+ to those hydrocarbons was energetically more favorable than for the other metal ions leaving more energy available for fragmentation. It is likely that the appearance of metal-containing fragments indicates that the metal ions have inserted into the polymer bonds. Only for the case (e.g., Fe)

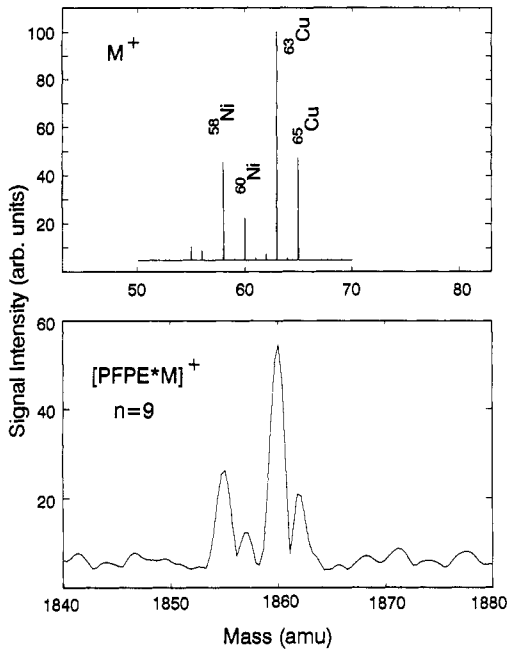

Figure 8. Comparison of relative efficiency for cationization of PFPEs by Cu^+ and Ni^+ ions: top trace, typical Cu^+, Ni^+ ion signals observed from ablation of Constantan (55% Cu, 45% Ni); bottom trace, cationized PFPE signal around 1860 amu ($n = 9$) from type I polymer on Constantan substrate. The peaks corresponding to the metal isotopes are labeled in the top trace.

where the energetics are favorable for further reaction would fragmentation be observed. The fact that the fragment complexes are metal-dependent supports the conclusion that they result from oxidative addition of the metal ions to the polymer after the initial complex formation, in accordance with the double well mechanism.[39]

C. Molecular Weight Distribution. We have applied this technique to determine the chain length distribution and average molecular weight of PFPE samples. There are other methods that can be used to determine average molecular weights such as HPLC and ^{19}F NMR. However, one gets limited information on the distribution of chain lengths or variations in the end groups of the polymer molecules from these methods. With laser desorption/cationization FTMS a more complete picture of a polymer sample, as shown by Figure 4, can be obtained.

The method for calculation of the average molecular weight of a polymer sample using FTMS has been described previously.[42,43] Each peak in a mass spectrum (such as Figure 4) corresponds to a given chain length and set of end groups. At the resolution used, each peak envelopes the distribution of isotopes associated with that species. To account for the change in resolution of FTMS with increasing mass and the change in the isotope distribution with increasing number of C-atoms, it is necessary to measure the area under each peak to obtain the relative amount of that species in a given sample. The assumption is made that the desorption efficiency remains constant for the different length PFPEs in a given sample. This appears to hold true for higher molecular weight samples ($m > 2000$) but not for those with molecular weights under ~2000. It is also assumed that there is no bias due to nonuniform excitation or detection of ions of different mass in the ICR cell.

The number average molecular weight, $\langle M \rangle$, is calculated according to

$$\langle M \rangle = \frac{\sum I_n M_n}{\sum I_n} \tag{5}$$

When using this equation with I_n equal to the area under each peak, we found that $\langle M \rangle$ came out higher than the values obtained

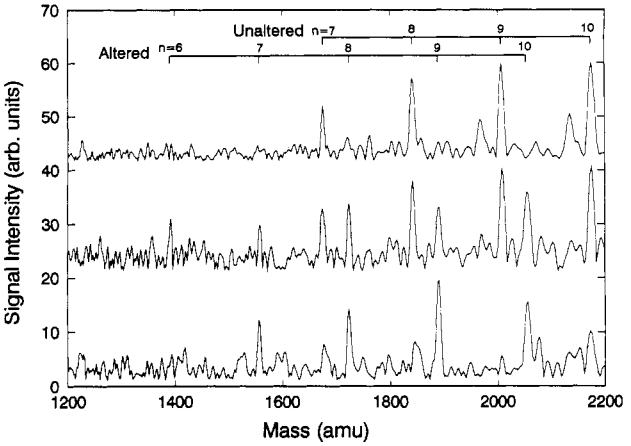

Figure 9. Portions of the mass spectrum of Cu^+-cationized SP polymer (III) exposed to various numbers of pulses of 248-nm laser radiation (0.8 mJ/pulse): top trace, unexposed sample area; middle trace, sample area exposed to 80 shots; bottom trace, sample area exposed to 320 shots. The region shown corresponds to chain lengths of $n = 7$ to 10. (Note that unaltered polymer m produces altered polymer $m - 1$). The complete spectrum extends from 1500 to 5000 amu (see Figure 10). The unaltered and altered PFPE peaks (discussed in text) are labeled.

TABLE I: Comparison of $\langle M \rangle$ Determined by FTMS and ^{19}F NMR

sample	FTMS	^{19}F
Demnum S65	4600 ± 85	4560 ± 50
Krytox 24	3970 ± 10	4030 ± 50

from ^{19}F NMR measurements. However, if one makes the simple assumption that the cationization cross section increases linearly with the polymer chain length

$$I_n = \frac{\text{area}(n)}{n} \tag{6}$$

a much better agreement results. This assumption is consistent with the cationization model discussed in section B. The average molecular weights calculated this way for two different polymer samples and the values obtained for the same samples using ^{19}F NMR are presented in Table I. The uncertainties in the $\langle M \rangle$ values determined by FTMS represent the standard deviation of five independent measurements. A Demnum S65 spectrum used to obtain the "FTMS" value is shown in Figure 4 while a Krytox 24 spectrum is shown in Figure 6. The agreement between the two methods is very good, attesting to the validity of using this method to determine chain length distributions of PFPE compounds.

D. Photochemistry. In the final part of this section we present an application of this technique to the study of chemical reactions. The polymer studied was a straight chain PFPE with a phenyl-containing end group, commercially available as Demnum SP, having structure III. Whereas the nonfunctionalized PFPE does not absorb at wavelengths above 200 nm, the addition of the phenyl group produces an absorption maximum at ~260 nm with significant absorption at 248 nm. This chromophore gives rise to photochemistry at 248 nm.

A mass spectrum of the SP film was taken with 20 laser shots at an energy of 3 mJ/pulse. At this exposure little change of the mass spectrum was observed while a good signal to noise ratio was obtained. Then areas of the sample were exposed to varying numbers of 248-nm pulses at reduced intensity (0.8 mJ/pulse) to avoid desorption, after which a mass spectrum was taken in the same manner as for the "unexposed" sample. Three of these spectra are shown in Figure 9: an unexposed area, an area exposed to 80 shots, and an area exposed to 320 shots. Only a portion of the spectra (from 1200 to 2200 amu) is shown in each case for sake of clarity.

The four main peaks in the top spectrum of Figure 9 correspond to unaltered SP polymer molecules of chain length $n = 7$ to 10 that have been cationized by Cu^+ ions. As the UV light interacts with the SP film, a second set of peaks appears (Figure 9, middle). These peaks, shifted down by 284 amu, are attributed to the formation of an acid fluoride end group, –CFO, at the first ether oxygen from the end according to the following overall reaction

$$R_1\text{–}(CF_2CF_2CF_2\text{–}O)_m\text{–}CF_2CF_2COO\text{–}CH_2CH_2\text{–}O\text{–}C_6H_5 \rightarrow R_1\text{–}(CF_2CF_2CF_2O)_{m-1}\text{–}CF_2CF_2CFO + CF_3CF_2COO\text{–}CH_2CH_2\text{–}O\text{–}C_6H_5 \quad (7)$$

The ion observed is the Cu^+-cationized acid fluoride. As the film is exposed to even more UV radiation, only the acid fluoride end groups are left in the mass spectrum (Figure 9, bottom).

This mechanism requires the cleavage to be specific to that single ether O since random breaking of the chain is not observed. Only one product is observed and its intensity in the mass spectrum is comparable to the parent intensity. This suggests that any other reaction pathways are minor. (No ions corresponding to the ester fragment were detected, possibly due to its high vapor pressure). Furthermore, no secondary dissociation of the polymer chain occurs. The distribution of chain lengths remains unchanged even after exposure to hundreds of shots beyond the amount necessary to completely remove all end groups. It should be noted that the acid fluoride reacts with water but is observable here because the photolysis is done in vacuum.

The reason why no secondary dissociation occurs appears to be the lack of significant absorption at 248 nm once the phenyl group is detached from the polymer. The same experiment described above was done with a 193-nm, ArF excimer laser desorbing the PFPE film. With the shorter wavelength the conversion of (III) to the acid fluoride happened on a much faster time scale (<50 shots UV). This is consistent with a higher absorption cross section for the polymer at 193 nm (as compared to 248 nm) and, possibly, a higher reaction probability (relative to relaxation processes). On further exposure to 193-nm radiation there was a continuing shift of the chain length distribution of the polymer toward lower mass. Since the normal PFPE (no chromophore) did not exhibit this behavior, the further degradation must be due to the absorption of 193-nm photons by the acid fluoride end group. This is followed by what seems to be a stepwise shortening of the chain length by cleavage at the closest ether oxygen to the chromophore resulting in the formation of another acid fluoride end group

$$R_1\text{–}(CF_2CF_2CF_2O)_nCF_2CF_2CFO \rightarrow R_1\text{–}(CF_2CF_2CF_2O)_{n-1}CF_2CF_2CFO + CF_3CF_2CFO \quad (8)$$

This chain shortening is shown in Figure 10. The top trace in Figure 10 shows the full distribution from Figure 9 (top) with no 193-nm exposure (the film was sampled with 20 shots of 248-nm light). The middle and bottom traces in Figure 10 show SP films which have been exposed to 100 and 800 shots of 193-nm laser light (0.5 mJ/pulse), respectively. Discussion of possible mechanisms for the end group removal (7) and chain shortening (8) reactions based on these results would be purely speculative. However, experiments are underway to provide insight into the mechanisms.

While the experiments reported above were all done in situ, other uses of this technique to study reactive processes are possible. Bulk polymer degradation could be examined by taking "before and after" mass spectra of a polymer subjected to some process. This would allow other causes of polymer degradation, such as thermal, mechanical, and electrical stresses, to be studied outside of a vacuum environment. Most methods used so far to look at such reactions have concentrated on detection of the smaller molecular weight species that are produced. This technique would be complementary to such studies, allowing detection of the higher molecular weight products and enabling a more complete characterization of polymer reactions.

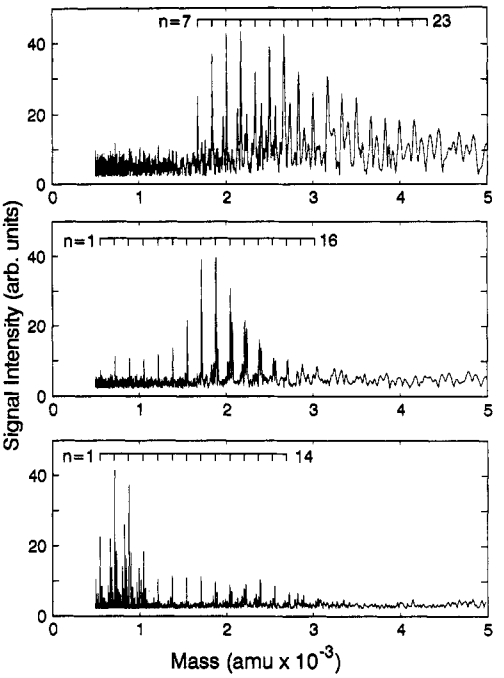

Figure 10. Mass spectrum of Cu^+-cationized SP polymer (III) exposed to 193-nm radiation: top trace, SP parent mass distribution spectrum taken using 248-nm desorption (see Figure 9, top trace) with no 193-nm exposure (labeled peaks correspond to cationized, intact SP polymer molecules); middle trace, mass spectrum after exposure to 100 pulses of 193-nm laser radiation (0.5 mJ/pulse); bottom trace, mass spectrum after exposure to 800 shots of 193-nm light. The labeled peaks in the bottom two spectra correspond to cationized polymers with acid fluoride end groups. A second group of peaks from ~1800 to ~3000 amu corresponds to cationized, nonfunctionalized PFPEs (type I) and is not affected by exposure to 193-nm light.

Summary

Cationization of organic compounds and hydrocarbon polymers with metal ions has been used successfully for many years. We have presented here a technique for observing perfluorinated compounds by transition-metal cationization with FTMS. The novel use of two lasers to separate the sample desorption and metal ion formation allows independent optimization of the two processes. This is important because different fluences are required for desorption and ablation. The method is relatively nondestructive to large molecules, producing mass spectra without significant fragmentation. This is a result both of the nature of the ionization process and of the polymer desorption process. The method has applications as a tool for analytical chemistry and for investigating reactive processes in surface films as well as bulk materials.

This technique has the advantage of using undoped samples, allowing the characterization of PFPE films on metal substrates. Sample preparation is minimized as compared to other techniques such as matrix-assisted desorption or alkali salt cationization. A disadvantage of this technique is that it is not very sensitive. We have obtained multishot spectra from 300 Å thick polymer films. With further optimization of the technique, we feel that detection limits can be lowered.

While the experiments described in this paper were all done with a film of PFPE on a metal substrate, other geometrical arrangements should also be possible. Close proximity of the PFPE and M^+ sources (0.1 mm or less) is necessary for high efficiency. However, it should be possible to generate the metal ion plume external to the surface on which the PFPEs (or other molecules) have been deposited. The restriction of the metal ions by the magnetic field must be considered.

Acknowledgment. The authors thank R. Johnson, G. Vurens, and Judy Lin for their help in providing samples and other information about the polymers used in this project.

References and Notes

(1) Burlingame, A. L.; Millington, D. S.; Norwood, D. L.; Russell, D. H. *Anal. Chem.* **1990**, *62*, 268R.
(2) Marshall, A. G.; Grosshans, P. B. *Anal. Chem.* **1991**, *63*, 215A.
(3) Lub, I.; van Vroonhove, F. C. B. M.; Brunix, E.; Benninghoven, A. *Polymer* **1989**, *30*, 40.
(4) Hillenkamp, F.; Karas, M.; Beavis, R. C.; Chait, B. T. *Anal. Chem.* **1991**, *63*, 1193A.
(5) Vertes, A.; Levine, R. D. *Chem. Phys. Lett.* **1990**, *171*, 284.
(6) van der Peyl, G. J. Q.; Isa, K.; Haverkamp, J.; Kistemaker, P. G. *Org. Mass Spectrom.* **1981**, *16*, 416.
(7) Johlman, C. L.; Wilkins, C. L.; Hogan, J. D.; Donovan, T. L.; Laude, D. A., Jr.; Youssefi, M.-J. *Anal. Chem.* **1990**, *62*, 1167.
(8) Llenes, C. F.; O'Malley, R. M. *Rapid Commun. Mass Spectrom.* **1992**, *6*, 564.
(9) Fowler, D. E.; Johnson, R. D.; vanLeyen, D.; Benninghoven, A. *Anal. Chem.* **1990**, *62*, 2088.
(10) Reihs, K.; Cromwell, E. F.; DeVries, M. S.; Wendt, H. R.; Ghaderi, S.; Hunziker, H. E. *Proc. 40th ASMS Conf. Mass Spec. May 31 - June 5* **1992**, 289.
(11) Lehman, T. A.; Bursey, M. M. *Ion Cyclotron Resonance Spectrometry; John Wiley & Sons: New York, 1976.*
(12) Wilkins, C. L.; Chowdhury, A. K.; Nuwaysir, L. M.; Coates, M. L. *Mass Spectrom. Rev.* **1989**, *8*, 67.
(13) Comisarow, M. B. *Int. J. Mass Spectrom. Ion Phys.* **1981**, *37*, 251.
(14) Yin, W. W.; Wang, M.; Marshall, A. G.; Ledford, E. B. *J. Am. Soc. Mass Spectrom.* **1992**, *3*, 188.
(15) Chen, L.; Wang, T.-C. L.; Ricca, T. L.; Marshall, A. G. *Anal. Chem.* **1987**, *59*, 449.
(16) Contact the authors for further information.
(17) Demnum is a registered tradename of Daikin Industries.
(18) Krytox is a registered tradename of E. I. du Pont de Nemours Co. (Wilmington, DE).
(19) Spyrou, S. M.; Sauers, I.; Christophorou, L. G. *J. Chem. Phys.* **1983**, *78*, 7200.
(20) Spyrou, S. M.; Hunter, S. R.; Christophorou, L. G. *J. Chem. Soc.* **1984**, *81*, 4481.
(21) Pacansky, J.; Waltman, R. J.; Wang, C. *J. Fluorine Chem.* **1986**, *32*, 283.
(22) Zakett, D.; Schoen, A. E.; Cooks, R. G.; Hemberger, P. H. *J. Am. Chem. Soc.* **1981**, *103*, 1295.
(23) Schmelzeisen-Redeker, B.; Giessmann, U.; Rollgen, F. W. *Org. Mass Spectrom.* **1985**, *20*, 305.
(24) Chiarelli, M. P.; Gross, M. L. *Int. J. Mass Spectrom. Ion Proc.* **1987**, *78*, 37.
(25) Hall, R. B. *J. Phys. Chem.* **1987**, *91*, 1007.
(26) van der Peyl, G. J. Q.; Haverkamp, J.; Kistemaker, P. G. *Int. J. Mass Spectrom. Ion Phys.* **1982**, *42*, 125.
(27) Srinivasan, R.; Braren, B.; Casey, K. G.; Yeh, M. *Appl. Phys. Lett.* **1989**, *55*, 2790.
(28) Leung, W. P.; Tam, A. C. *Appl. Phys. Lett.* **1992**, *60*, 23.
(29) Singh, R. K.; Nargan, J. *Phys. Rev. B* **1990**, *41*, 8843.
(30) Halle, L. F.; Armentrout, P. B.; Beauchamp, J. L. *Organometallics* **1983**, *2*, 1829.
(31) Eller, K.; Schwarz, H. *Chem. Rev.* **1991**, *91*, 1121.
(32) Armentrout, P. B. *Annu. Rev. Phys. Chem.* **1990**, *41*, 313.
(33) Halle, L. F.; Crowe, W. E.; Armentrout, P. B.; Beauchamp, J. L. *Organometallics* **1984**, *3*, 1694.
(34) van Koppen, P. A. M.; Brodbelt-Lustig, J.; Bowers, M. T.; Dearden, D. V.; Beauchamp, J. L.; Fisher, E. R.; Armentrout, P. B. *J. Am. Chem. Soc.* **1991**, *113*, 2359.
(35) Pacansky, J.; Miller, M.; Hatton, W.; Liu, B.; Scheiner, A.; Waltman, R. *J. Am. Chem. Soc.* **1991**, *113*, 329. Waltman, R.; Pacanski, J., private communication.
(36) Kasai, P. H.; Wheeler, P. *Appl. Surf. Sci.* **1992**, *52*, 91.
(37) Su, T.; Bowers, M. T. *Gas Phase Ion Chemistry*; Academic Press: New York, 1979; Vol. 1.
(38) Longevialle, P. *Mass Spectrom. Rev.* **1992**, *11*, 157.
(39) Moylan, C. R.; Brauman, J. I. In *Dynamics of Ion-Molecule Complexes*; Hase, W. L., Ed.; JAI Press, in press. Moylan, C. R.; Brauman, J. I. *IBM Res. Rep.* **1991**, *RJ 8256*.
(40) Burnier, R. C.; Byrd, G. D.; Freiser, B. S. *J. Am. Chem. Soc.* **1981**, *103*, 4360.
(41) Halle, L. F.; Armentrout, P. B.; Beauchamp, J. L. *Organometallics* **1982**, *1*, 963.
(42) Brown, R. S.; Weil, D. A.; Wilkins, C. L. *Macromolecules* **1986**, *19*, 1255.
(43) Nuwaysir, L. M.; Wilkins, C. L. *Anal. Chem.* **1988**, *60*, 279.